mathematics

MDPI

Article

Periodic Solutions and Stability Analysis for Two-Coupled-Oscillator Structure in Optics of Chiral Molecules

Jing Li [1,*], Yuying Chen [1] and Shaotao Zhu [1,2,*]

[1] Interdisciplinary Research Institute, Faculty of Science, Beijing University of Technology, Beijing 100124, China; cyy2017@emails.bjut.edu.cn
[2] Faculty of Information Technology, Beijing University of Technology, Beijing 100124, China
* Correspondence: leejing@bjut.edu.cn (J.L.); zhushaotao@bjut.edu.cn (S.Z.)

Abstract: Chirality is an indispensable geometric property in the world that has become invariably interlocked with life. The main goal of this paper is to study the nonlinear dynamic behavior and periodic vibration characteristic of a two-coupled-oscillator model in the optics of chiral molecules. We systematically discuss the stability and local dynamic behavior of the system with two pairs of identical conjugate complex eigenvalues. In particular, the existence and number of periodic solutions are investigated by establishing the curvilinear coordinate and constructing a Poincaré map to improve the Melnikov function. Then, we verify the accuracy of the theoretical analysis by numerical simulations, and take a comprehensive look at the nonlinear response of multiple periodic motion under certain conditions. The results might be of important significance for the vibration control, safety stability and design optimization for chiral molecules.

Keywords: chiral molecules; two-coupled-oscillator model; bifurcation; stability analysis; periodic solutions

MSC: 37G15; 37J46

check for updates

Citation: Li, J.; Chen, Y.; Zhu, S. Periodic Solutions and Stability Analysis for Two-Coupled-Oscillator Structure in Optics Chiral Molecular. *Mathematics* **2022**, *10*, 1908. https://doi.org/10.3390/math10111908

Academic Editor: Magdalena Toda

Received: 13 April 2022
Accepted: 27 May 2022
Published: 2 June 2022

Publisher's Note: MDPI stays neutral with regard to jurisdictional claims in published maps and institutional affiliations.

Copyright: © 2022 by the authors. Licensee MDPI, Basel, Switzerland. This article is an open access article distributed under the terms and conditions of the Creative Commons Attribution (CC BY) license (https://creativecommons.org/licenses/by/4.0/).

1. Introduction

Chirality is the basic attribute of nature, existing in all levels of macro and micro matter ubiquitously. Similar to our left hand and right hand, it is a mirror image of each other and cannot overlap. Life substances such as proteins, nucleic acids and their components can manifest chiral optical activity [1]. In 1848, Louis Pasteur separated the left-handed and right-handed sodium ammonium tartrate crystals and observed the optical isomerism of molecules in the crystal solution [2,3]. This made scientists have more conceptions about the exploration of chirality and the development of stereochemistry, which is the charm of asymmetry. With the deepgoing extension of the chiral field, it was found that chiral recognition of different enantiomers sometimes varies greatly. As for L-dopamine, which treats Parkinson's disease, it is produced by decarboxylase acting on the left-handed enantiomers of L-dopa, whereas its right-handed enantiomers cannot be metabolized and have the risk of deposition. Racemization thalidomide, once used as a sedative and antiemetic agent, caused serious disaster due to the (S)-isomer with teratogenicity [4,5]. The research on the property mechanism and state analysis of chiral compounds and chiral molecules has also become a common concern of physicists, chemists, biologists and even pharmaceutical scientists.

There are three typical molecular models for the research on the nonlinearity of chiral molecules: the spiral single electron model is used for the chiral molecules with a helical micro-structure or their valence electron moving along the helical path [6,7]; the two-coupled-oscillator model is described as two charged oscillators moving orthogonally on two parallel planes at a certain distance and having an elastic weak coupling interaction [8–10]; the three-coupled-oscillator model refers to a tripod-like structure composed of a chiral center and three different groups that can be regarded as spring

oscillators [11]. Scholars have investigated the nonlinear effects of these three models in terms of polarizability, hyperpolarizability and second harmonic generation. As for the two-coupled-oscillator model, Yin et al. realized its exact plasmonic analog through experiments and adjusted the vertical distance between corner-stacked gold nanorods to discuss the excitation mode [9]. Gui et al. studied the third-harmonic circular dichroism of a typical oscillator model by means of chiral plasmonic metasurfaces and explored the nonlinear chiroptical response of such chiral structures [12]. From the deeper perspective of physics, the two-coupled-oscillator model in the optics of chiral molecules is commonly discussed regarding light transmission through dense solutions and dense ordered aggregates of chiral DNA molecules. The manifestation of this model can be understood, as the DNA base tends to assemble into pairs through hydrogen bonds and is interconnected into a double helix structure. Considering the interactions between groups, the attachment points allow for a more compact and solid packing through rotating [13]. Moreover, the various states of strand coupling and strand separation, deformation and compaction in the DNA make the study of this model interesting [14,15]. It is widely used to describe and rationalize the dynamics of the DNA and other structures with the same properties. We strive to provide useful references for the further exploration of chiral molecules in various fields, and our research might pave the way toward nonlinear dynamics of a two-coupled-oscillator system evolving with time, including analyzing the stability and discussing the periodic motion state.

The stability of motion originates from mechanics. In 1788, Lagrange proposed a general theorem on the stability of equilibrium, which was proven by Dirichlet [16]. In 1877, Routh offered an inspection method for the stability of the linear system. Hurwitz gave the stability criterion in 1894 [17,18]. Until 1892, Lyapunov creatively presented the strict mathematical definition of stability, and put forward the method to solve the problem of stability, which laid the foundation of theory [19,20]. With the continuous research of scholars and need of the vibration control theory, the exploration of motion stability has gradually developed from finite dimensional space to infinite dimensional space, and from the field of mechanics to mechanical engineering, aerospace, material chemical and other fields [21–23]. Furthermore, the research on stability analysis has been applied to various models. Hategekimana et al. analyzed the local and global asymptotic stability of epidemic models by using Routh–Hurwitz criterion and the Lyapunov direct method [24]. Zhang et al. discussed the stability and bifurcation conditions of a predator–prey system with the weak Allee effect [25]. Meanwhile, the research on periodic solutions and bifurcations of high-dimensional complex nonlinear dynamic systems closely related to Hilbert's 16th problem is of great significance in solving practical scientific problems [26]. The nonlinear dynamics have been greatly permeated into various systems, such as the isochronous center system and Hamilton system from theoretical analysis and numerical simulation [27,28]. Barreira et al. demonstrated upper bounds for the number of periodic solutions generated by the bifurcation of a 1:N resonance center system using average theory [29]. Afterwards, the first-order averaging theory was used to investigate the limit cycles of zero-Hopf singularity bifurcation on C^{m+1} differential systems [30]. Sun et al. proposed a subharmonic Melnikov function to determine the existence of subharmonic orbits for a four-dimensional degenerate resonance non-autonomous system and applied it to a honeycomb sandwich plate [31]. Kadry et al. estimated the number of periodic solutions of first-order ordinary differential equations by the derived numbers method [32]. Li et al. obtained sufficient and necessary conditions for the existence of periodic solutions of a class non-autonomous slow–fast system [33].

This overall structure is shown as follows. In Sections 2 and 3, the two-coupled-oscillator model in the optics of chiral molecules and a four-dimensional average equation in rectangular coordinates are presented. In Section 4, we demonstrate the trajectories and time series graphs of phase space by determining the parameters in stable and unstable regions. In Section 5, the number and relative position of periodic solutions are reflected

intuitively by theoretical analysis and numerical simulation. In Section 6, we describe the characteristics of multiple periodic motions. In Section 7, conclusions are given.

2. Model and System of Two-Coupled-Oscillator Structure

A class of chiral molecules have the following characteristics: there are two spatially separated but mutually coupled charged groups, and the positive as well as negative charge centers of groups do not superpose. The vibration under an external field force results in the nonlinearity of two-coupled-oscillator structure molecules (as shown in Figure 1).

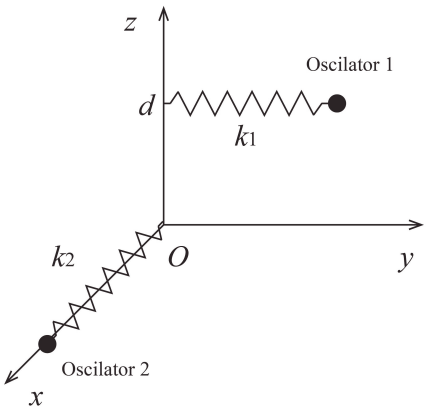


Figure 1. The two-coupled-oscillator model in optics of chiral molecules.

We focus on the two-coupled-oscillator model in the optics of chiral molecules, which can be described by the following two degrees of freedom nonlinear dynamic system:

$$\begin{aligned}\ddot{w}_i + 2\gamma\dot{w}_i + \omega_i^2 w_i + k_i\cos(\Omega_2 t)w_i + \alpha_1 w_{3-i} + \alpha_{2,i}w_i^2 + \alpha_{3,i}w_{3-i}^2 \\ + 2\alpha_{3,3-i}w_i w_{3-i} + \alpha_{4,i}w_i^3 - \alpha_5 w_{3-i}^3 + \alpha_6 w_{3-i}^2 w_i - \alpha_7 w_i^2 w_{3-i} = f_i\cos(\Omega_1 t)\end{aligned} \tag{1}$$

where $i = 1, 2$, w_i are the displacement of two oscillators away from the equilibrium position. γ represents the damping coefficient. ω_i are natural vibration frequencies.

$$\omega_i^2 = (k_i + k_3 a_0^{4-2i} b_0^{2i-2})/m, a_0 = x_0/l_0, b_0 = y_0/l_0, l_0 = \sqrt{x_0^2 + y_0^2 + d^2}$$

k_i denote the elastic coefficients of oscillator 1 and oscillator 2, respectively. k_3 is the coupling elastic coefficient and m is mass. x_0 and y_0 are intrinsic lengths in x and y directions when two oscillators are kept in the equilibrium position. l_0 represents the spacing. d is the vertical space distance of two oscillators in the z axis. f_i denotes the Cartesian component function of the incident electric field. Ω_i is the electric field excitation frequency. Other non-dimensional parameters are defined as

$$\alpha_1 = k_3 a_0 b_0/m, \alpha_{2,i} = 3k_3 a_0^{2-i} b_0^{i-1}(1 - a_0^{4-2i} b_0^{2i-2})/2ml_0$$

$$\alpha_{3,i} = k_3 a_0^{2-i} b_0^{i-1}(1 - 3a_0^{2i-2} b_0^{4-2i})/2ml_0, \alpha_{4,i} = k_3(1 - 6a_0^{4-2i} b_0^{2i-2})/2ml_0^2$$

$$\alpha_6 = k_3(1 - 3a_0^2 - 3b_0^2)/2ml_0^2, \alpha_7 = 9k_3 a_0 b_0/2ml_0^2 = 3\alpha_5$$

3. Average Equation of Two-Coupled-Oscillator Structure

Considering a 1:1 internal resonance for the two-coupled-oscillator structure, the resonant relations are given as follows:

$$\omega_i^2 = \Omega_i^2 + \varepsilon\sigma_i \tag{2}$$

where σ_i are two detuning parameters and ε is a small parameter. In order to apply the method of multiple scales, the scale transformations for variables may be introduced as

$$\gamma \to \varepsilon\gamma, k_i \to \varepsilon k_i, f_i \to \varepsilon f_i, \alpha_1 \to \varepsilon\alpha_1, \alpha_{2,i} \to \varepsilon\alpha_{2,i}$$

$$\alpha_{3,i} \to \varepsilon\alpha_{3,i}, \alpha_{4,i} \to \varepsilon\alpha_{4,i}, \alpha_5 \to \varepsilon\alpha_5, \alpha_6 \to \varepsilon\alpha_6, \alpha_7 \to \varepsilon\alpha_7$$

Assume that the approximate solutions of uniform asymptotic series for variables w_i are

$$w_i = \sum_{j=0}^{+\infty} \varepsilon^j w_{ij}(T_0, T_1, T_2) \tag{3}$$

where $T_s = \varepsilon^s t (s = 0, 1, 2)$. The series expression of the time differential operator in the upper expression is

$$\frac{\mathrm{d}}{\mathrm{d}t} = \sum_{j=0}^{+\infty} \frac{\partial}{\partial T_j}\frac{\partial T_j}{\partial t} = \sum_{j=0}^{+\infty} \varepsilon^j D_j, \frac{\mathrm{d}^2}{\mathrm{d}t^2} = (\sum_{j=0}^{+\infty} \varepsilon^j D_j)^2 = D_0^2 + 2\varepsilon D_0 D_1 + \cdots \tag{4}$$

where $D_j = \partial/\partial T_j$. Introducing Equations (2)–(4) into Equation (1) and balancing the coefficients of perturbation parameter ε on both sides of equation with the same order, we have

ε^0 order

$$D_0^2 w_{i0} + w_{i0} = 0 \tag{5}$$

ε^1 order

$$\begin{aligned} D_0^2 w_{i1} + w_{i1} = &- k_i w_{i0}\cos t - \alpha_1 w_{(3-i)0} - \alpha_{2,i} w_{i0}^2 - \alpha_{3,i} w_{(3-i)0}^2 - 2\alpha_{3,3-i} w_{i0} w_{(3-i)0} \\ &- \alpha_{4,i} w_{i0}^3 + \alpha_5 w_{(3-i)0}^3 - \alpha_6 w_{i0} w_{(3-i)0}^2 + \alpha_7 w_{i0}^2 w_{(3-i)0} - 2\gamma D_0 w_{i0} \\ &+ f_i \cos t - \sigma_i w_{i0} - 2D_0 D_1 w_{i0} \end{aligned} \tag{6}$$

ε^2 order

$$\begin{aligned} D_0^2 w_{i2} + w_{i2} = &- k_i w_{i1}\cos t - \alpha_1 w_{(3-i)1} - 2\alpha_{2,i} w_{i0} w_{i1} - 2\alpha_{3,i} w_{(3-i)0} w_{(3-i)1} \\ &- 2\alpha_{3,3-i}(w_{i0} w_{(3-i)1} + w_{i1} w_{(3-i)0}) - 3\alpha_{4,i} w_{i0}^2 w_{i1} + 3\alpha_5 w_{(3-i)0}^2 w_{(3-i)1} \\ &- \alpha_6(2w_{i0} w_{(3-i)0} w_{(3-i)1} + w_{i1} w_{(3-i)0}^2) + \alpha_7(2w_{i0} w_{i1} w_{(3-i)0} \\ &+ w_{i0}^2 w_{(3-i)1}) - 2\gamma(D_0 w_{i1} + D_1 w_{i0}) - \sigma_i w_{i1} - 2D_0 D_1 w_{i1} \\ &- 2D_0 D_2 w_{i0} - D_1^2 w_{i0} \end{aligned} \tag{7}$$

The solutions of Equation (5) in the complex form are expressed as

$$w_{i0} = A_i(T_1, T_2) e^{\mathrm{i}T_0} + \bar{A}_i(T_1, T_2) e^{-\mathrm{i}T_0} \tag{8}$$

where $\bar{A}_i$ are conjugate parts of A_i. After substituting Equation (8) into Equation (6) and eliminating the secular term form, we obtain

$$\begin{aligned} D_1 A_i = &- \gamma A_i - \frac{\mathrm{i}}{4} f_i + \frac{\mathrm{i}}{2}\sigma_i A_i + \frac{\mathrm{i}}{2}\alpha_1 A_{3-i} + \frac{3\mathrm{i}}{2}\alpha_{4,i} A_i^2 \bar{A}_i - \frac{3\mathrm{i}}{2}\alpha_5 A_{3-i}^2 \bar{A}_{3-i} \\ &+ \frac{\mathrm{i}}{2}\alpha_6 \bar{A}_i A_{3-i}^2 + i\alpha_6 A_i A_{3-i} \bar{A}_{3-i} - \frac{\mathrm{i}}{2}\alpha_7 A_i^2 \bar{A}_{3-i} - i\alpha_7 A_i \bar{A}_i A_{3-i} \end{aligned} \tag{9}$$

The special solutions of Equation (6) are

$$\begin{aligned} w_{i1} =& \frac{1}{8}e^{3\mathrm{i}T_0}\cdot(\alpha_{4,i}A_i^3-\alpha_5A_{3-i}^3+\alpha_6A_iA_{3-i}^2-\alpha_7A_i^2A_{3-i})+\frac{1}{3}e^{2\mathrm{i}T_0}\cdot(\alpha_{2,i}A_i^2 \\ &+2\alpha_{3,3-i}A_iA_{3-i}+\alpha_{3,i}A_{3-i}^2+\frac{1}{2}k_iA_i)-\frac{1}{2}k_i(A_i+\bar{A}_i)-2(\alpha_{2,i}A_i\bar{A}_i \\ &+\alpha_{3,1}A_{3-i}\bar{A}_{3-i}+\alpha_{3,3-i}A_i\bar{A}_{3-i}+\alpha_{3,3-i}\bar{A}_iA_{3-i})+cc \end{aligned} \tag{10}$$

where cc represents the complex conjugate part of the function on the right-hand side of Equation (9). Substituting Equation (9) into Equation (7) and eliminating the secular term, we obtain

$$\begin{aligned} D_2A_i =& \frac{\mathrm{i}}{16}(\sigma_if_i+\alpha_1f_{3-i}-2\mathrm{i}\gamma f_i)-\frac{\mathrm{i}}{8}(\sigma_i^2+\alpha_1^2+4\gamma^2-16a_{0,i})A_i+3\mathrm{i}a_{0,i}\bar{A}_i \\ &-\frac{\mathrm{i}}{2}(a_{4,i}+a_{5,i}-a_{6,i})A_{3-i}^2-\frac{\mathrm{i}}{3}(9a_{6,3-i}+3a_{7,i}+a_{9,i})A_iA_{3-i} \\ &-\frac{\mathrm{i}}{3}(9a_{6,3-i}-3a_{7,i}+a_{9,i})A_i\bar{A}_{3-i}+\mathrm{i}(a_{6,3-i}+a_{7,i}-a_{9,i})\bar{A}_iA_{3-i} \\ &-\mathrm{i}a_1A_{3-i}-\frac{\mathrm{i}}{2}(a_{2,i}+a_{3,i})A_i^2-\frac{\mathrm{i}}{3}(a_{5,i}-3a_{4,i}+9a_{6,i})A_{3-i}\bar{A}_{3-i} \\ &+\mathrm{i}(a_{2,i}-a_{3,i})A_i\bar{A}_i+(\frac{1}{2}a_{14}+\frac{\mathrm{i}}{3}(3a_{24,i}-9a_{23,i}-5a_{22,i}))A_i^2\bar{A}_{3-i} \\ &+(a_{10,i}+\mathrm{i}a_{11,i})A_i^2\bar{A}_i+(\frac{1}{2}a_{13}+\mathrm{i}(\frac{1}{3}a_{17}+3a_{18}-\frac{1}{2}a_{20,i}-a_{21}-2a_{16}))\bar{A}_iA_{3-i}^2 \\ &+(a_{12}-\mathrm{i}a_{15,i})A_{3-i}^2\bar{A}_{3-i}+(a_{14}-2\mathrm{i}(a_{23,i}+a_{24,i}+\frac{5}{3}a_{22,i}))A_iA_{3-i}\bar{A}_i \\ &+(a_{13}+2\mathrm{i}(a_{18}+a_{21}-\frac{2}{3}a_{16}-a_{17}-\frac{1}{2}a_{19,i}))A_iA_{3-i}\bar{A}_{3-i} \end{aligned} \tag{11}$$

If we let A_i be of the following form

$$A_i(T_1,T_2)=x_{2i-1}(T_1,T_2)+\mathrm{i}x_{2i}(T_1,T_2) \tag{12}$$

then the four-dimensional average equation in Cartesian form is obtained by using the methods of multiple scales:

$$\dot{\boldsymbol{x}}=\boldsymbol{L}\boldsymbol{x}+\boldsymbol{X}(\boldsymbol{x}) \tag{13}$$

where $\boldsymbol{x}=(x_1,x_2,x_3,x_4)^{\mathrm{T}}\in\mathbf{R}^4,\boldsymbol{X}=(g_1,l_1,g_2,l_2)^{\mathrm{T}}$ is the vector valued polynomials in variables of $x_n(n=1,\cdots,4)$. The specific expressions of g_i and l_i are shown in the appendices. $\boldsymbol{L}$ is the matrix and can be shown as

$$\boldsymbol{L}=\sum_{i=1}^{2}(\partial_{2i-1,2i}^{4,4}-\partial_{2i,2i-1}^{4,4})m_i,m_i=\frac{1}{8}\alpha_1^2+\frac{1}{2}\gamma^2+\frac{1}{8}\sigma_i^2$$

$\partial_{p,q}^{u,v}(\boldsymbol{M})$ denotes a $u\times v$ block matrix with a (p,q)-th block $\boldsymbol{M}$, and all other blocks are zero matrices [34].

4. Stability Analysis

Motion stability is used to explore the influence of the disturbance force on the motion state of the system, so as to establish the criterion for judging whether the motion performance is stable. Generally, if the disturbance is imposed on dynamic systems at a time in the process of stable motion, even small factors will affect the motion state. For some systems, this effect is gradually attenuated after a period of time, making the difference between the disturbed and undisturbed motion very minimal. Such motion can be called stable. On the contrary, this kind of influence becomes obvious with an increase in time. Even if it is a small disturbance, the disturbed motion is far from the undisturbed motion, which is called unstable.

This section mainly deduces the properties of the solution according to the characteristics of the differential equation to judge the motion behavior from the perspective of qualitative analysis. This provides some reference for finding the number and relative position of periodic solutions in the next section. Normally, the nonzero equilibrium in differential equations can be transformed into a zero solution equilibrium by the coordinate translation principle. Therefore, we only need to consider the stability near the zero solution equilibrium point. $E_0 = (0, 0, 0, 0)$ is the equilibrium point of the four-dimensional average equation. The characteristic polynomial corresponding to the system can be written as

$$f(\lambda) = \sum_{r=0}^{4} \beta_r \lambda^{4-r} = \lambda^4 + 4\gamma\lambda^3 + (\frac{1}{4}\sigma_1^2 + \frac{1}{4}\sigma_2^2 + \frac{1}{2}\alpha_1^2 + 6\gamma^2)\lambda^2 + (\frac{1}{2}\sigma_1^2 + \frac{1}{2}\sigma_2^2 + \alpha_1^2 + 4\gamma^2)\gamma\lambda + \frac{1}{4}\gamma^2(\sigma_1^2 + \sigma_2^2 + 2\alpha_1^2 + 4\gamma^2) + \frac{1}{16}(\sigma_1\sigma_2 - \alpha_1^2)^2 \tag{14}$$

In this section, the case of two pairs of identical conjugate complex eigenvalues being in the characteristic polynomial is discussed at the equilibrium point. When selecting tuning parameters, we consider a relationship of 1:1 internal resonance so that $\sigma_1 = \sigma_2$ for convenience of analysis. The perturbation parameter γ is introduced into perturbation transformation. According to the Routh–Hurwitz criterion, the conditions for the stability of the initial solution at the equilibrium point can be obtained, so as to judge the stable region and unstable region.

In order to verify the validity of theoretical analysis and discuss the trajectory distribution near the equilibrium point, we numerically analyze the four-dimensional average equation to acquire stable and unstable trajectories. As shown in Figure 2a, we can see that the trajectory is a counterclockwise spiral line around point E_0. It gradually tends to the equilibrium point from the initial point in helical form from outside to inside and reaches a stable state. As shown in Figure 2b, the trajectory is also a helix line that rotates counterclockwise and surrounds equilibrium point E_0. Nevertheless, the difference is that the trajectory gradually moves away from inside to outside, and it is in an unstable state. Therefore, the equilibrium point E_0 is determined as the focus. Figure 3 shows the phase portraits of the (x_1, x_2) plane in different intervals of stable and unstable regions. The (x_3, x_4) plane is similar. This perceives the movement trend and orientation of the system more intuitively.

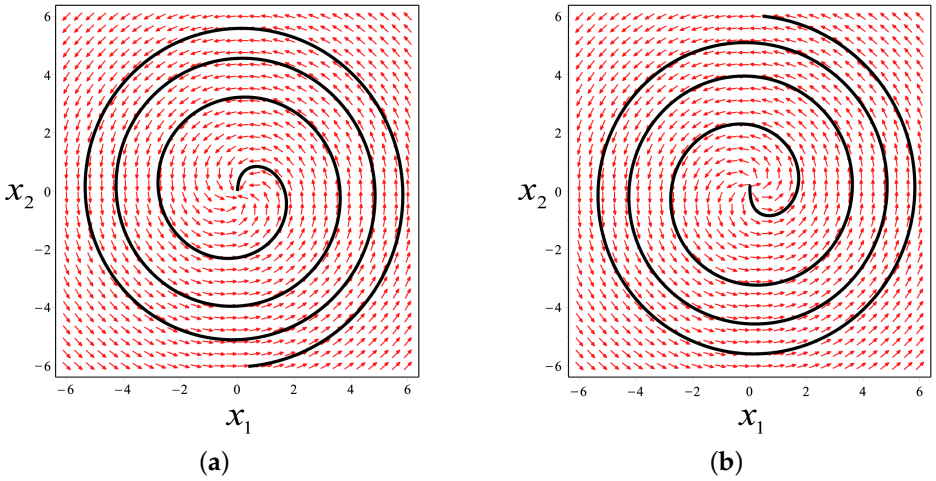


Figure 2. Trajectories on (x_1, x_2) plane: (**a**) Stable region; (**b**) Unstable region.

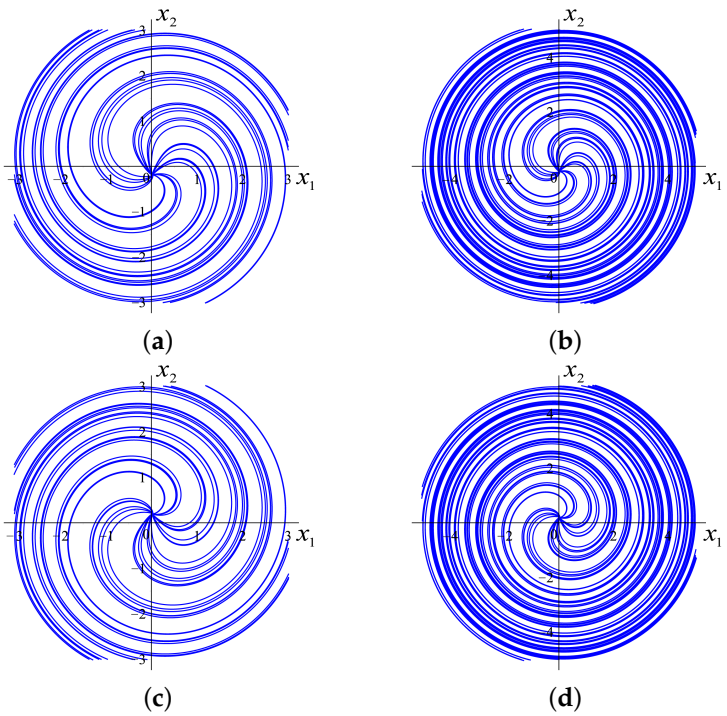


Figure 3. Phase portraits of (x_1, x_2) plane: (**a**) Stable region ($x_i \in [-3, 3]$); (**b**) Stable region $x_i \in [-5, 5]$); (**c**) Unstable region ($x_i \in [-3, 3]$); (**d**) Unstable region ($x_i \in [-5, 5]$).

By drawing the time series graphs, we can observe the overall change in trend of elastic oscillators under the action of internal resonance factors for a long time and show the non-stationary variation, such as waves fluctuation. As shown in Figure 4, x_1 in Figure 4a tends to zero with time t increasing, that is, it approaches the equilibrium point and appears as peaks or troughs alternately. Figure 4b shows the trend and direction of x_1 over time in the unstable region. With the increase in time t, the vibration amplitude presents a continuous rise, fall or no change in the same nature, and the change amplitude may be different. The time series graphs further verify the one-to-one correspondence between time and phase portraits. This section only presents part of the graphs; other direction or plane graphs can be obtained similarly through the four-dimensional nonlinear average equation.

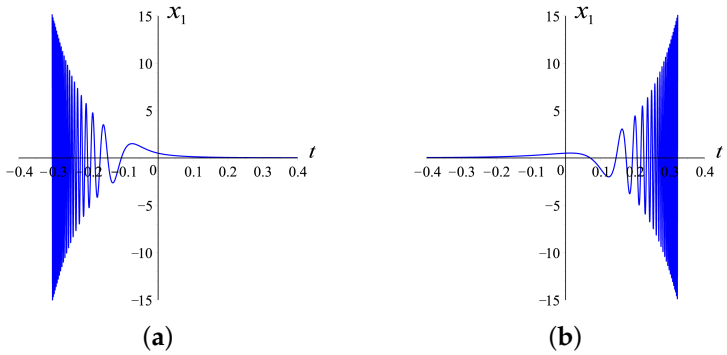


Figure 4. Time series graphs of x_1 direction: (**a**) Stable region; (**b**) Unstable region.

5. Existence and Bifurcation Conditions of Periodic Solutions

5.1. Transformations and Melnikov Function for the System

Introducing the rescaling transformations $\boldsymbol{X}(\boldsymbol{x}) \to \varepsilon \boldsymbol{X}(\boldsymbol{x})$ and considering when $\varepsilon = 0$, System (13) degenerates into two decoupling nonlinear Hamiltonian systems with Hamiltonian functions

$$H_i(x_{2i-1}, x_{2i}) = \frac{1}{2} m_i (x_{2i-1}^2 + x_{2i}^2)$$

Each system has a family of periodic orbits

$$\Gamma_{h_i} = \{\boldsymbol{x}_{h_i} | H_i(x_{2i-1}, x_{2i}) = h_i\}$$

on planes (x_1, x_2) and (x_3, x_4), which can be expressed as

$$x_1 = \sqrt{\frac{2h_1}{m_1}}\cos(m_1 t), x_2 = \sqrt{\frac{2h_1}{m_1}}\sin(m_1 t)$$

$$x_3 = \sqrt{\frac{2h_2}{m_2}}\cos(m_2(t+t_0)), x_4 = \sqrt{\frac{2h_2}{m_2}}\sin(m_2(t+t_0))$$

The periods of the orbits are $T_i(h_i) = 2\pi/m_i$.

In order to construct the Poincaré map, we introduced curvilinear coordinates in a sufficiently small neighborhood of Γ_h and established a curvilinear coordinate frame. A global cross section Σ in phase space was defined and the k-th iteration $p^k : \Sigma \to \Sigma$ of Poincaré map was constructed. The fixed point of p^k corresponds to the periodic solution of system. It can be obtained by calculating the zero point of the improved Melnikov function $\boldsymbol{M} = (M_1, M_2, M_3)^{\mathrm{T}}$, where

$$M_1 = m_1 \int_0^{2\pi} (x_1 \cdot g_1 + x_2 \cdot l_1)\mathrm{d}t, M_2 = m_2 \int_0^{2\pi} (x_3 \cdot g_2 + x_4 \cdot l_2)\mathrm{d}t$$

$$M_3 = \int_0^{2\pi} \frac{(x_4 g_2 - x_3 l_2)h_1 - (x_2 g_1 - x_1 l_1)h_2}{2h_1 h_2}\mathrm{d}t$$

Let $\boldsymbol{M} = 0$ and $m_2 = 2m_1 = 2$, $T_1(h_1) = 2T_2(h_2) = 2\pi$; then,

$$M_1 = 2a_{10,1}h_1^2 + a_{13}h_1 h_2 - c_1 h_1\sqrt{h_2}\sin(2t_0) = 0 \tag{15a}$$

$$M_2 = a_{10,2}h_2^2 + 2a_{13}h_1 h_2 - c_2 h_1\sqrt{h_2}\sin(2t_0) = 0 \tag{15b}$$

$$M_3 = c_4 h_1 + c_5 h_2 + (c_2 h_1 + 2c_1 h_2)\cos(2t_0)/4\sqrt{h_2} + c_3 = 0 \tag{15c}$$

where

$$c_1 = a_{7,1} + a_{8,1} - a_{9,1}, c_2 = a_{4,2} + a_{5,2} - a_{6,2}, c_3 = a_{0,1} - \frac{1}{2}a_{0,2}$$

$$c_4 = a_{11,1} + \frac{2}{3}a_{16} + a_{17} - a_{18} + \frac{1}{2}a_{19,2} - a_{21}, c_5 = -\frac{1}{4}a_{11,2} - \frac{2}{3}a_{16} - a_{17} + a_{18} - \frac{1}{2}a_{19,1} + a_{21}$$

Assuming that $h_1 = \xi h_2 (\xi > 0)$, the following solution can be obtained from (15a) and (15b):

$$\sqrt{h_1} = \sqrt{\xi h_2} = \rho\sqrt{\xi}\sin(2t_0), \sqrt{h_2} = \rho\sin(2t_0) \tag{16}$$

Substitute (16) into (15c) and obtain

$$\varphi(\sin^2(2t_0)) = (A^2 + B^2)\sin^4(2t_0) - (B^2 - 2AC)\sin^2(2t_0) + C^2 = 0 \tag{17}$$

where A and B are functions of ξ and ρ. We can see $\varphi(\sin^2(2t_0))$ as a quadratic equation of $\sin^2(2t_0)$. Therefore, the number of periodic solutions of the system can be found by discussing the number of solutions for (h_1, h_2, t_0) in Formula (17).

5.2. Bifurcation and Control of Periodic Solutions

In order to understand the nonlinear dynamic properties of the two-coupled-oscillator structure more intuitively, we investigate the influence of f_1 on the number and relative positions of periodic orbits and select a group of fixed parameters conditions for numerical simulation with the assumption of $a_{7,1} = 0$, $a_{8,1} = a_{9,1}$, $a_{5,2} = a_{6,2}$.

$$\begin{aligned} UP &= (\gamma, k_1, k_2, \alpha_1, \alpha_{2,1}, \alpha_{2,2}, \alpha_{3,1}, \alpha_{3,2}, \alpha_{4,1}, \alpha_{4,2}, \alpha_5, \alpha_6, \alpha_7) \\ &= (1, 1, 6, \sqrt{3}, \frac{1}{2}, -1, -1, 1, -\frac{1}{8}, 4, 1, 5, 5) \end{aligned}$$

If $A^2 + B^2 \neq 0$, $B^2 - AC \neq 0$ and $C \neq 0$, Equation (17) becomes a quadratic equation of $\sin^2(2t_0)$ with $\triangle = B^2(B^2 - 4C^2 - 4AC)$, and the image of function $\triangle$ is shown in Figure 5. When $\triangle = 0$, there are three solutions: 0, f_{11} and f_{12}.

$$f_{12} = -f_{11} = \frac{1}{10}\sqrt{4743 + 153\sqrt{3} + 17\sqrt{252808 + 5022\sqrt{3}}}$$

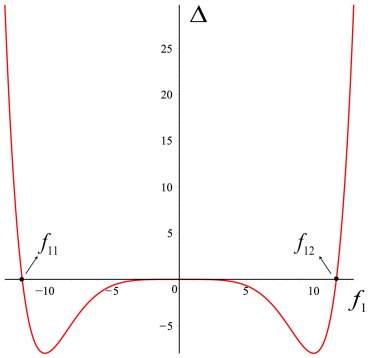


Figure 5. The image of function $\triangle$ with respect to f_1 under condition UP.

(1) When $f_1 < f_{11}$ or $f_1 > f_{12}$, we have $\triangle > 0$ and there are two solutions for $\sin^2(2t_0)$. The periodic solutions of the system appear in pairs. According to the relationship between roots and coefficients, the system has four periodic solutions for (h_1, h_2, t_0). We divide them into two pairs, Γ^+ and Γ^-, which satisfy

$$\Gamma^+ = \{\boldsymbol{x} | h_i = \xi^{2-i}\rho^2 \frac{(B^2 - 2AC) + \sqrt{\triangle}}{2(A^2 + B^2)}\}, \Gamma^- = \{\boldsymbol{x} | h_i = \xi^{2-i}\rho^2 \frac{(B^2 - 2AC) - \sqrt{\triangle}}{2(A^2 + B^2)}\}$$

(2) When $f_1 = f_{11}$ or $f_1 = f_{12}$, we have $\triangle = 0$ and there is only one solution for $\sin^2(2t_0)$. The system has two periodic solutions for (h_1, h_2, t_0). Two pairs of periodic orbits coincide, forming one pair of periodic orbits at the critical point $f_1 = f_{11}$ or $f_1 = f_{12}$, which satisfies

$$\Gamma^0 = \{\boldsymbol{x} | h_i = \xi^{2-i}\rho^2 \frac{B^2 - 2AC}{2(A^2 + B^2)}\}$$

(3) When $f_{11} < f_1 < f_{12}$ and $f_1 \neq 0$, we have $\triangle < 0$ and there is no real solution for $\sin^2(2t_0)$. The system has no periodic solutions.

5.3. Numerical Simulation

The existence of periodic solutions and the process of bifurcation are explained by theoretical analysis. In order to understand the morphology and relative position change in periodic motions for the system more intuitively, we select the perturbation parameter $\varepsilon = 0.000001$ in the situations below for numerical simulation, and draw the phase portraits in plane and space, which vividly illustrate the influence of f_1 on the relative positions and the number of solutions for the system.

(1) When $f_1 = 15 > f_{12}$, there are four periodic solutions that can be divided into two pairs:

$$\Gamma^+ = \{\boldsymbol{x} | h_1 = 0.8328860790, h_2 = 0.06246645595\}$$
$$\Gamma^- = \{\boldsymbol{x} | h_1 = 0.05897221862, h_2 = 0.004422916398\}$$

Figure 6 demonstrates the morphology and relative positions of periodic orbits for the system. The periodic orbits Γ^+ have a bigger amplitude and the periodic orbits Γ^- have a smaller amplitude. Figure 6a–c denote the phase portraits of periodic orbits projected on two-dimensional planes. It can be seen that the projections of two pairs of periodic orbits Γ^+ and Γ^- coincide in the same pair on the (x_1, x_2), (x_1, x_3), (x_2, x_3) and (x_3, x_4) planes. Figure 6d–f show the phase portraits of periodic orbits projected in a three-dimensional space. Furthermore, the moving morphology of the periodic orbit in Γ^+ is a one-to-one correspondence with that in Γ^-.

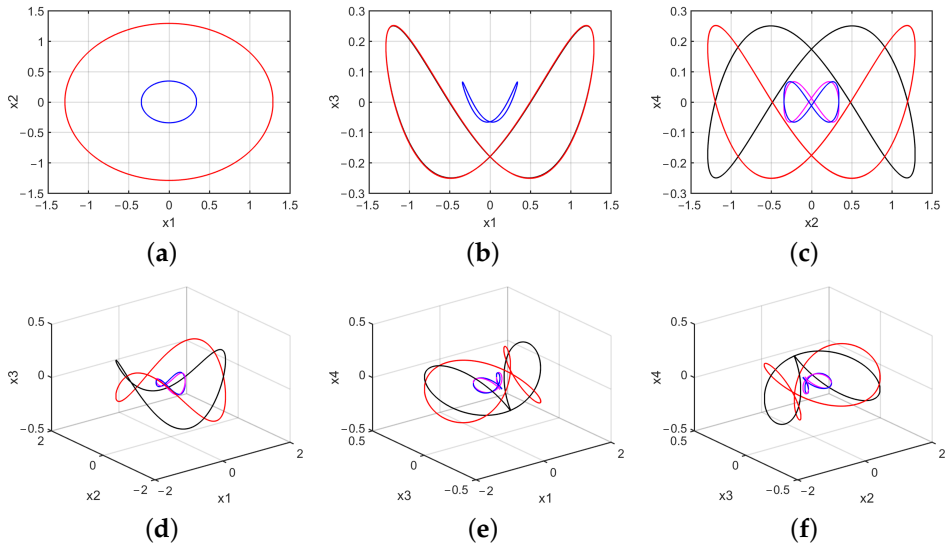


Figure 6. Morphology and relative positions of four periodic solutions when $f_1 = 15 > f_{12}$: (**a**) (x_1, x_2) plane; (**b**) (x_1, x_3) plane; (**c**) (x_2, x_4) plane; (**d**) (x_1, x_2, x_3) space; (**e**) (x_1, x_3, x_4) space; (**f**) (x_2, x_3, x_4) space.

(2) When $f_1 = 13 > f_{12}$, there are four periodic solutions, which can be divided into two pairs:

$$\Gamma^+ = \{\boldsymbol{x} | h_1 = 0.5100307424, h_2 = 0.03825230570\}$$
$$\Gamma^- = \{\boldsymbol{x} | h_1 = 0.09630231245, h_2 = 0.007222673439\}$$

Figure 7 demonstrates the morphology and relative positions of periodic orbits. Compared with Situation (1), the amplitude of the periodic orbit in Γ^+ is decreasing and the amplitude of the periodic orbit in Γ^- is increasing, which indicates that two pairs of periodic orbits are slowly approaching each other.

(3) When $f_1 = 12 > f_{12}$, there are four periodic solutions, which can be divided into two pairs:

$$\Gamma^+ = \{\boldsymbol{x} | h_1 = 0.3300484682, h_2 = 0.02475363512\}$$
$$\Gamma^- = \{\boldsymbol{x} | h_1 = 0.1488179606, h_2 = 0.01116134705\}$$

It can be seen from Situation (1) and Situation (2) that, when the value of $f_1 = 15$ decreases to $f_1 = 13$, the relative positions of two pairs of periodic orbits changes, that is, they are slowly approaching. In order to further verify whether the periodic motion continues in this way, we selected $f_1 = 12$ to obtain the phase portraits describing the morphology and relative positions of periodic motions for the system as shown in Figure 8. It is confirmed that two pairs of periodic orbits Γ^+ and Γ^- tend to approach and may coincide with each other when the value of f_1 decreases.

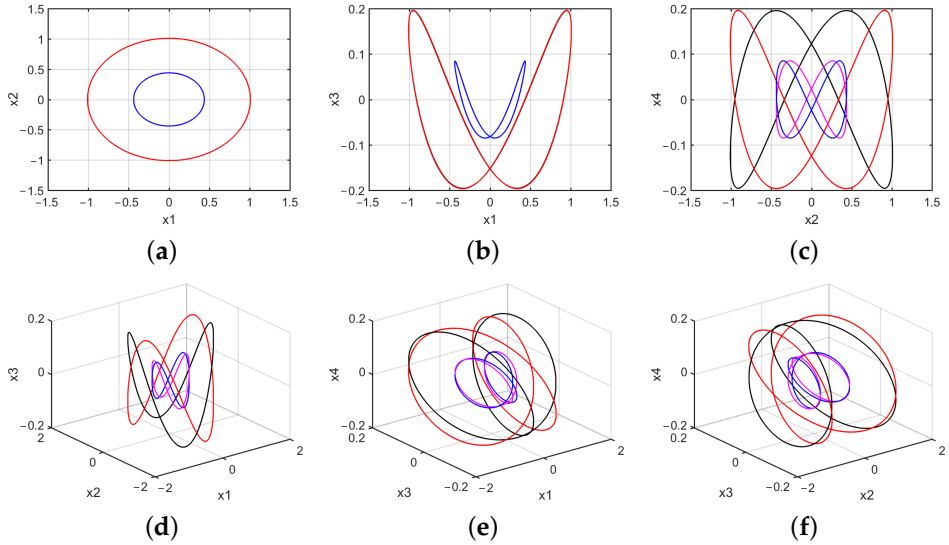


Figure 7. Morphology and relative positions of four periodic solutions when $f_1 = 13 > f_{12}$: (**a**) (x_1, x_2) plane; (**b**) (x_1, x_3) plane; (**c**) (x_2, x_4) plane; (**d**) (x_1, x_2, x_3) space; (**e**) (x_1, x_3, x_4) space; (**f**) (x_2, x_3, x_4) space.

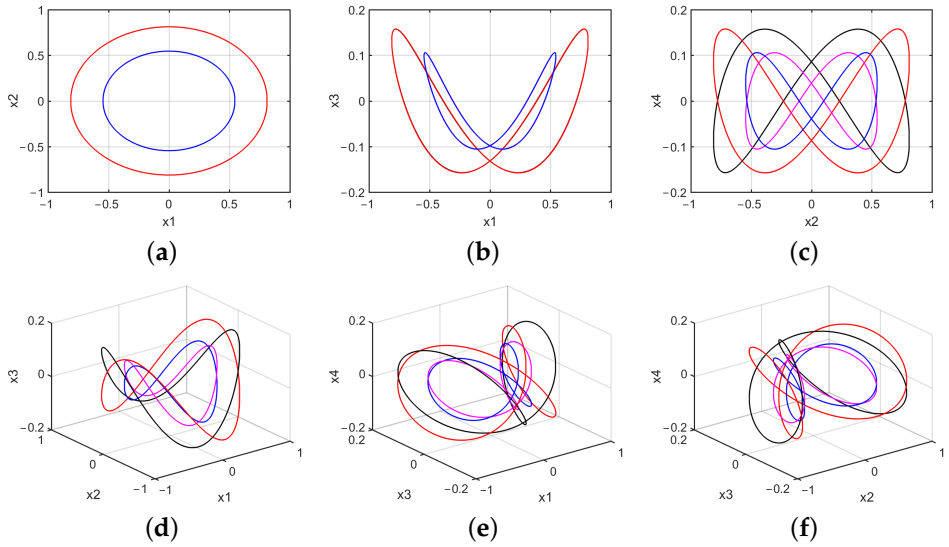


Figure 8. Morphology and relative positions of four periodic solutions when $f_1 = 12 > f_{12}$: (**a**) (x_1, x_2) plane; (**b**) (x_1, x_3) plane; (**c**) (x_2, x_4) plane; (**d**) (x_1, x_2, x_3) space; (**e**) (x_1, x_3, x_4) space; (**f**) (x_2, x_3, x_4) space.

(4) When $f_1 = f_{12}$, the bifurcation of the system produces a pair of periodic trajectories that satisfy $\Gamma^0 = \{\boldsymbol{x} | h_1 = 0.2216238705, h_2 = 0.01662179029\}$. The morphology of periodic motion and the relative positions are shown in Figure 9. We observe that the phase portraits projected on the (x_1, x_2) plane and (x_3, x_4) plane have changed from two central symmetry closed trajectories to one, and the phase portraits in space have changed from four closed orbits to two. This directly shows that the system bifurcation occurs at $f_1 = f_{12}$ and that the original two pairs of periodic orbits coincide into a pair of periodic orbits.

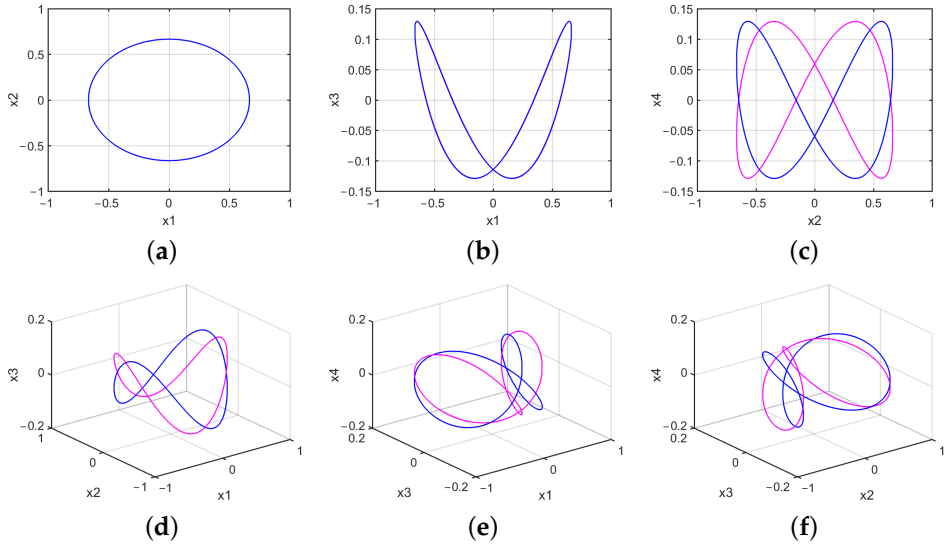


Figure 9. Morphology and relative positions of two periodic solutions when $f_1 = f_{12}$: **(a)** (x_1, x_2) plane; **(b)** (x_1, x_3) plane; **(c)** (x_2, x_4) plane; **(d)** (x_1, x_2, x_3) space; **(e)** (x_1, x_3, x_4) space; **(f)** (x_2, x_3, x_4) space.

(5) When $f_1 < f_{12}$, there is no periodic solution for the system. The phase portraits in the plane and space are shown in Figure 10. The solution curve is densely distributed, circling like butterfly wings, but without closed orbits. In life, we can see a similar curve morphology, which is an interesting phenomenon.

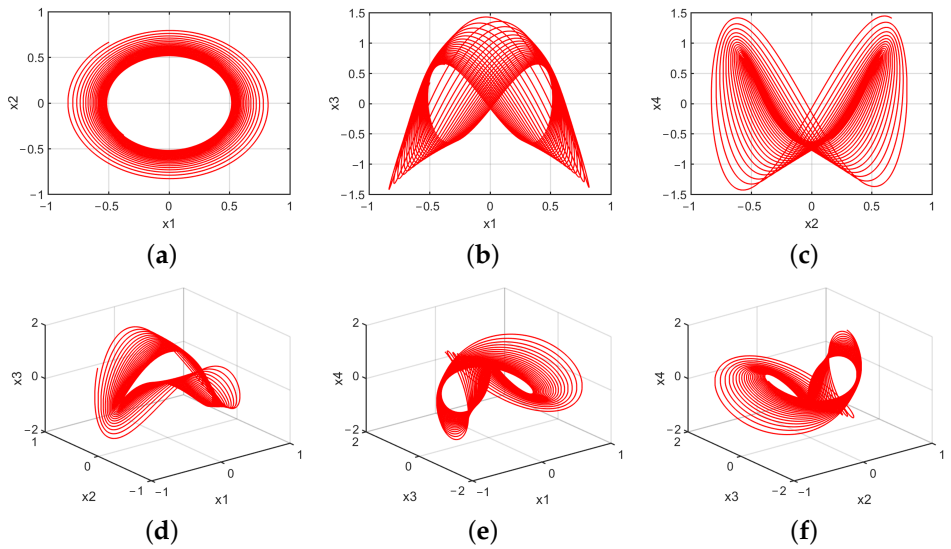


Figure 10. Phase portraits of the orbits (no periodic solution) when $f_1 < f_{12}$: **(a)** (x_1, x_2) plane; **(b)** (x_1, x_3) plane; **(c)** (x_2, x_4) plane; **(d)** (x_1, x_2, x_3) space; **(e)** (x_1, x_3, x_4) space; **(f)** (x_2, x_3, x_4) space.

From the above situations, we analyze the specific changes in bifurcation when f_1 crosses f_{12} from right to left. Since f_{11} and f_{12} have symmetric properties, this change will also occur when f_1 passes through f_{11}. We use the (x_1, x_2, f_1) space to describe the whole process (as show in Figure 11). When $f_1 > f_{12}$, there exists two pairs of periodic orbits that have a one-to-one correspondence with each other. With the decreases in parameter f_1, the amplitude of periodic orbits in Γ^+ gradually decreases and the amplitude of periodic orbits in Γ^- gradually increases, that is, they are slowly approaching. The phenomenon of coincidence occurs at the bifurcation value $f_1 = f_{12}$, forming a pair of periodic orbits Γ^0, and then disappears when $f_1 < f_{12}$. The bifurcation behavior can also be described in

the same way at $f_1 < 0$. The only difference is that the bifurcation direction of $f_1 < 0$ is different from that of $f_1 > 0$. A pair of periodic orbits are generated at $f_1 = f_{11}$, which is immediately split into two pairs of periodic orbits when f_1 decreases and passes through f_{11} from right to left. Throughout the process, the bifurcation of periodic solutions occurs twice; the corresponding bifurcation values are $f_1 = f_{11}$ and $f_1 = f_{12}$, respectively.

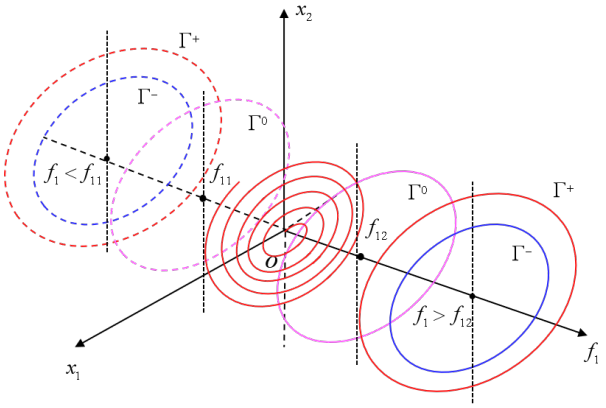


Figure 11. Bifurcation of periodic orbits in (x_1, x_2, f_1) space.

6. Multiple Periodic Motion of Two-Coupled-Oscillator Structure

Periodic motion can reflect the motion characteristics of the system under certain conditions. It describes the specific behavior over a certain time. From the types of periodic motion development at present, it can be found that quasi-periodic motion, almost periodic motion and multiple periodic motion are motion modes with great research value. The nonlinear dynamic behavior of the system is discussed from multiple perspectives, which also provides more possibilities for the application of the two-coupled-oscillator model in the field of chiral molecules.

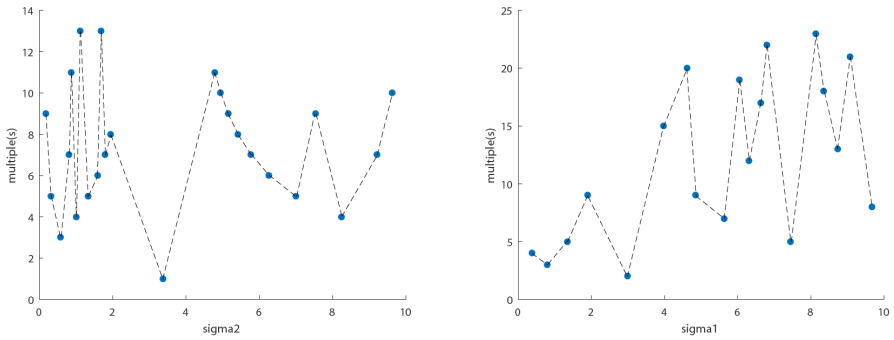
We set the initial condition $(x_1, x_2, x_3, x_4) = (0, 0.2, 0.12, 0.1)$ and selected σ_2 as the free parameter to investigate the influence of σ_2 on the nonlinear dynamic behavior of the system. As shown in Table 1, multiple periodic motions occur due to the change in σ_2 in the system within the range $[0, 10]$, and different multiple periodic motions are obtained corresponding to specific values. In the range of $[0, 10]$, periodic motions appear at 24 specific values. We obtained the minimum onefold periodic motion at $\sigma_2 = 3.3647$ and the maximum thirteenfold periodic motion at $\sigma_2 = 1.1199$ and $\sigma_2 = 1.6884$. It can be seen intuitively from Figure 12a that the multiple of periodic motion does not change regularly with the increase in σ_2, but changes in a jumping manner. When discussing the influence of different parameters on system motion in practical application, it is necessary to analyze the change in trajectory according to specific parameters. Table 2 shows the multiples of periodic motions that occur under the same initial conditions by fixing the value of σ_2 and adjusting the value of σ_1 within the range of $[0, 10]$. We obtained the minimum twofold periodic motion at $\sigma_1 = 3.9801$ and the maximum twenty-three-fold periodic motion at $\sigma_1 = 8.1412$. It can be observed that the system is more likely to have motion multiples of more than 13 cycles under the change in parameter σ_1 from Figure 12b. When σ_2 is selected as a free parameter, the periodic motion occurs more in the first half of the range. For parameter σ_1, the periodic motion caused by its value change occurs more in the latter half of the range. Therefore, the system of a two-coupled-oscillator is relatively sensitive to parameter changes and always switches back and forth between periodic motions with different multiples.

Table 1. Multiples of periodic motion with parameter σ_2.

Number	σ_2	Multiple (s)	Number	σ_2	Multiple (s)
1	0.1690	9	13	3.3647	1
2	0.3124	5	14	4.7810	11
3	0.5716	3	15	4.9431	10
4	0.8002	7	16	5.1468	9
5	0.8702	11	17	5.4095	8
6	1.0011	4	18	5.7615	7
7	1.1199	13	19	6.2567	6
8	1.3292	5	20	7.0009	5
9	1.5833	6	21	7.5314	9
10	1.6884	13	22	8.2368	4
11	1.7826	7	23	9.2085	7
12	1.9433	8	24	9.6206	10

Table 2. Multiples of periodic motion with parameter σ_1.

Number	σ_1	Multiple (s)	Number	σ_1	Multiple (s)
1	0.3811	4	11	6.3116	12
2	0.7983	3	12	6.6229	17
3	1.3432	5	13	6.8000	22
4	1.8987	9	14	7.4486	5
5	2.9801	2	15	8.1412	23
6	3.9695	15	16	8.3480	18
7	4.6103	20	17	8.7295	13
8	4.8512	9	18	9.0724	21
9	5.6284	7	19	9.6648	8
10	6.0491	19			



(**a**) (**b**)

Figure 12. The scatter plots between multiple periods and free parameter: (**a**) Free parameter σ_2; (**b**) Free parameter σ_1.

From the data sheets and scatter plots, we can know the specific value of σ_2 corresponding to the occurrence of multiple periodic motion. In the following, we analyze the motion state of the system according to the plane and three-dimensional phase portraits of periodic motions with different multiples. Taking periodic-3 motion of $\sigma_2 = 0.5716$ as an example (as shown in Figure 13), the phase portrait in the (x_1, x_2, x_3) coordinate is composed of circling and closed trajectories. We take a point a as the initial point on the track, and reach the point b on the same vertical line when rotating around the trajectory for one week. Similarly, when rotating the third circle, the moving point on the trajectory will return to the initial point a, which is triple periodic motion. It can be found from the (x_1, x_3) plane phase portrait that, when the vertical line on the x_1 axis moves to the intersection of two lines (only in the case of an intersection), three intersections will appear (as shown in Figure 13b), that is, the triple periodic motion is explained again. The planar

and three-dimensional phase portraits for other cases of parameters σ_1 and σ_2 are shown in Appendix A. These graphs can help to understand the meaning of multiple periodic motion more comprehensively.

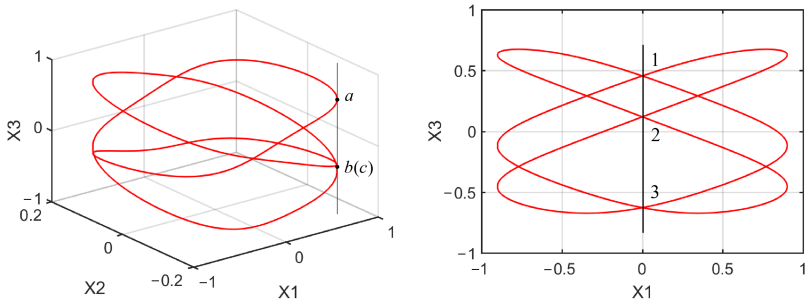


Figure 13. Periodic-3 motion of $\sigma_1 = 0.67$, $\sigma_2 = 0.5716$: **(a)** (x_1, x_2, x_3) space; **(b)** (x_1, x_3) plane.

7. Conclusions

Due to the weak elastic coupling interaction between two oscillators, there are many internal resonance cases in the high-dimensional nonlinear system. This paper mainly realizes and discusses the nonlinear vibration behavior and parameter control of a chiral molecular two-coupled-oscillator model under a 1:1 internal resonance. According to the nonlinear transformation and Routh–Hurwitz criterion, the stability and local dynamic behavior of the system with two pairs of identical conjugate complex eigenvalues, as well as the trajectories and time series graphs of phase space, are investigated in detail by selecting parameters in stable and unstable regions. At the same time, we aim to retrieve the existence and number of periodic solutions by establishing the curvilinear coordinate and constructing a Poincaré map to improve the Melnikov function. Taking f_1 as a bifurcation parameter, it is determined that $f_1 = f_{11}$ and $f_1 = f_{12}$ are two critical values for the bifurcation of periodic orbits. In addition, our research pays close attention to the relative position of multiple periodic motion by numerical analysis, which can intuitively reflect the response of different parameters on system motion in practical application.

The existence, number upper bound and distribution configuration of multiple periodic solutions for high-dimensional nonlinear dynamic systems are hot issues in the current international research field of nonlinear dynamics and control. As is well known, the two-oscillator model may induce a resonance phenomenon under the coupling effect. It is necessary to study the structural state during resonance in order to solve practical problems. For the motion equation that cannot be directly solved, it is a new way to select the periodic solution theory to discuss the existence and stability of periodic orbits. This paper breaks the limitation of traditional mathematical methods, such as the center manifold theory in dimension reduction and the geometric structure description of high-dimensional nonlinear dynamical systems. The approach determines the existence and number of periodic solutions and makes the distribution configuration more intuitive by numerical simulation. This is the novelty from the mathematical or fundamental perspective. In this paper, the specific analysis combined with an optical chiral molecules nonlinear model is of great significance to the vibration control, safety stability and optimized design of the system. In the meantime, it was found in the literature that some scholars work on the nonlinearity of chiral nanostructures according to the Born–Kuhn type bilayer chiral metasurfaces. These studies on the most basic chiral plasmon structure provide tools for analyzing and understanding natural optical activity. It will be important to simplify the problem by considering the combination of real physical phenomena and multiple parameters. From this point of view, the further development of theoretical analysis and numerical calculation in this paper will promote the attention and innovation of periodic solutions for high-dimensional nonlinear dynamical systems in interdisciplinary fields, and will be directly applied to a broader platform.

Author Contributions: Conceptualization, J.L.; Formal analysis, Y.C. and S.Z.; Funding acquisition, J.L.; Investigation, Y.C.; Methodology, J.L.; Project administration, J.L.; Supervision, J.L.; Validation, S.Z. Visualization, Y.C.; Writing—original draft, Y.C.; Writing—review & editing, S.Z. All authors contributed equally to this research. All authors have read and agreed to the published version of the manuscript.

Funding: The research project is supported by National Natural Science Foundation of China (11772007) and also supported by Beijing Natural Science Foundation (1172002, Z180005).

Institutional Review Board Statement: Not applicable.

Informed Consent Statement: Not applicable.

Data Availability Statement: Not applicable.

Conflicts of Interest: The authors declare no conflict of interest.

Appendix A

Appendix A.1. The Average Equation and Notations

Table A1. Notations adopted in average equation.

$a_{0,i} = -k_i^2/24$	$a_1 = (\alpha_1\sigma_1 + \alpha_1\sigma_2)/8$	$a_{2,i} = (3\alpha_{4,i}f_i - \alpha_7 f_{3-i})/8$
$a_{3,i} = 5k_i\alpha_{2,i}/6$	$a_{4,i} = (-3\alpha_5 f_{3-i} + \alpha_6 f_i)/8$	$a_{5,i} = k_{3-i}\alpha_{3,i}$
$a_{6,i} = k_i\alpha_{3,i}/6$	$a_{7,i} = (\alpha_6 f_{3-i} - \alpha_7 f_i)/8$	$a_{8,i} = k_{3-i}\alpha_{3,3-i}/6$
$a_{9,i} = k_i\alpha_{3,3-i}$	$a_{10,i} = 3\gamma\alpha_{4,i}/2$	$a_{12} = -3\gamma\alpha_5/2$
$a_{13} = \gamma\alpha_6$	$a_{14} = -\gamma\alpha_7$	$a_{16} = \alpha_{3,1}^2 + \alpha_{3,2}^2$
$a_{17} = \alpha_{3,2}\alpha_{2,2} + \alpha_{2,1}\alpha_{3,1}$	$a_{18} = \alpha_1\alpha_7/8$	$a_{19,i} = \alpha_6\sigma_i/2$
$a_{20,i} = \alpha_6\sigma_{3-i}/2$	$a_{21} = 3\alpha_1\alpha_5/8$	$a_{22,i} = \alpha_{2,i}\alpha_{3,3-i} + \alpha_{3,1}\alpha_{3,2}$
$a_{23,i} = (\alpha_1\alpha_6 - \alpha_7\sigma_i)/8$	$a_{24,i} = (3\alpha_1\alpha_{4,i} - \alpha_7\sigma_{3-i})/8$	$a_{25,i} = \gamma f_i/8$
$a_{26,i} = (\sigma_i f_i + \alpha_1 f_{3-i})/16$	$a_{11,i} = (\alpha_1\alpha_7 + 3\alpha_1\alpha_5)/8 - 5(\alpha_{2,i}^2 + \alpha_{3,3-i}^2)/3 - 3\alpha_{4,i}\sigma_i/4$	
$a_{15,i} = [-3(\alpha_5\sigma_{3-i} - \alpha_1\alpha_{4,3-i} + \alpha_5\sigma_i) + \alpha_1\alpha_6]/8 + 5(\alpha_{3,i}\alpha_{2,3-i} + \alpha_{3,1}\alpha_{3,2})/3$		

Appendix A.2. The Four-Dimensional Average Equation

$$
\begin{aligned}
g_i = {} & a_{0,i}x_{2i} + a_1x_{6-2i} + (a_{2,i} + a_{3,i})x_{2i-1}x_{2i} + (a_{4,i} + a_{5,i} - a_{6,i})x_{5-2i}x_{6-2i} + a_{7,i}(x_{2i}x_{5-2i} \\
& + x_{2i-1}x_{6-2i}) + a_{8,i}(7x_{2i}x_{5-2i} - x_{2i-1}x_{6-2i}) + a_{9,i}(x_{2i-1}x_{6-2i} - x_{2i}x_{5-2i}/3) + a_{10,i}(x_{2i-1}^3 \\
& + x_{2i-1}x_{2i}^2) - a_{11,i}(x_{2i}^3 + x_{2i-1}^2x_{2i}) + a_{12}(x_{5-2i}x_{6-2i}^2 + x_{5-2i}^3) + a_{13}(3x_{2i-1}x_{5-2i}^2/2 \\
& + x_{2i-1}x_{6-2i}^2/2 + x_{2i}x_{5-2i}x_{6-2i}) + a_{14}(3x_{2i-1}^2x_{5-2i}/2 + x_{2i}^2x_{5-2i}/2 + x_{2i-1}x_{2i}x_{6-2i}) \\
& + a_{15,i}(x_{6-2i}^3 + x_{5-2i}^2x_{6-2i}) + a_{16}(-2x_{2i}x_{5-2i}^2/3 + 10x_{2i}x_{6-2i}^2/3 + 4x_{2i-1}x_{5-2i}x_{6-2i}) \\
& + a_{17}(7x_{2i}x_{5-2i}^2 + 5x_{2i}x_{6-2i}^2 - 2x_{2i-1}x_{5-2i}x_{6-2i})/3 + a_{18}(x_{2i}x_{5-2i}^2 - 5x_{2i}x_{6-2i}^2 \\
& - 6x_{2i-1}x_{5-2i}x_{6-2i}) + a_{19,i}(x_{2i}x_{6-2i}^2 + x_{2i}x_{5-2i}^2) + a_{20,i}(-x_{2i}x_{5-2i}^2/2 + x_{2i}x_{6-2i}^2/2 \\
& + x_{2i-1}x_{5-2i}x_{6-2i}) + a_{21}(-3x_{2i}x_{5-2i}^2 - x_{2i}x_{6-2i}^2 + 2x_{2i-1}x_{5-2i}x_{6-2i}) + a_{22,i}(5x_{2i}^2x_{6-2i} \\
& + 5x_{2i-1}^2x_{6-2i}/3 + 10x_{2i-1}x_{2i}x_{5-2i}/3) + a_{23,i}(-x_{2i-1}^2x_{6-2i} + 5x_{2i}^2x_{6-2i} + 6x_{2i-1}x_{2i}x_{5-2i}) \\
& + a_{24,i}(3x_{2i-1}^2x_{6-2i} + x_{2i}^2x_{6-2i} - 2x_{2i-1}x_{2i}x_{5-2i}) + a_{25,i}
\end{aligned}
$$

$$
\begin{aligned}
l_i = {} & 5a_{0,i}x_{2i-1} - a_1x_{5-2i} + a_{2,i}(x_{2i-1}^2 + 3x_{2i}^2)/2 - a_{3,i}(3x_{2i-1}^2 + x_{2i}^2)/2 + a_{4,i}(x_{5-2i}^2 + 3x_{6-2i}^2)/2 \\
& + a_{5,i}(-5x_{5-2i}^2 + x_{6-2i}^2)/6 - a_{6,i}(5x_{5-2i}^2 + 7x_{6-2i}^2)/2 + a_{7,i}(3x_{2i}x_{6-2i} + x_{2i-1}x_{5-2i}) \\
& + a_{8,i}(x_{2i}x_{6-2i} - 5x_{2i-1}x_{5-2i}) - a_{9,i}(x_{2i}x_{6-2i} + 5x_{2i-1}x_{5-2i}/3) + a_{10,i}(x_{2i}^3 + x_{2i-1}^2x_{2i}) \\
& + a_{11,i}(x_{2i-1}^3 + x_{2i-1}x_{2i}^2) + a_{12}(x_{6-2i}^3 + x_{5-2i}^2x_{6-2i}) + a_{13}(x_{2i}x_{5-2i}^2/2 + 3x_{2i}x_{6-2i}^2/2 \\
& + x_{2i-1}x_{5-2i}x_{6-2i}) + a_{14}(x_{2i-1}^2x_{6-2i}/2 + 3x_{2i}^2x_{6-2i}/2 + x_{2i-1}x_{2i}x_{5-2i}) - a_{15,i}(x_{5-2i}^3 \\
& + x_{5-2i}x_{6-2i}^2) + a_{16}(-10x_{2i-1}x_{5-2i}^2/3 + 2x_{2i-1}x_{6-2i}^2/3 - 4x_{2i}x_{5-2i}x_{6-2i}) + a_{17}(-5x_{2i-1}x_{5-2i}^2 \\
& - 7x_{2i-1}x_{6-2i}^2 + 2x_{2i}x_{5-2i}x_{6-2i})/3 + a_{18}(5x_{2i-1}x_{5-2i}^2 - x_{2i-1}x_{6-2i}^2 + 6x_{2i}x_{5-2i}x_{6-2i}) \\
& - a_{19,i}(x_{2i-1}x_{6-2i}^2 + x_{2i-1}x_{5-2i}^2) + a_{20,i}(-x_{2i-1}x_{5-2i}^2/2 + x_{2i-1}x_{6-2i}^2/2 - x_{2i}x_{5-2i}x_{6-2i}) \\
& + a_{21}(x_{2i-1}x_{5-2i}^2 + 3x_{2i-1}x_{6-2i}^2 - 2x_{2i}x_{5-2i}x_{6-2i}) - a_{22,i}(5x_{2i-1}^2x_{5-2i} + 5x_{2i}^2x_{5-2i}/3 \\
& + 10x_{2i-1}x_{2i}x_{6-2i}/3) + a_{23,i}(-5x_{2i-1}^2x_{5-2i} + x_{2i}^2x_{5-2i} - 6x_{2i-1}x_{2i}x_{6-2i}) \\
& + a_{24,i}(2x_{2i-1}x_{2i}x_{6-2i} - x_{2i-1}^2x_{5-2i} - 3x_{2i}^2x_{5-2i}) + a_{26,i}
\end{aligned}
$$

Appendix A.3. Multiple Periodic Motions when σ_2 Is the Free Parameter ($\sigma_1 = 0.67$)

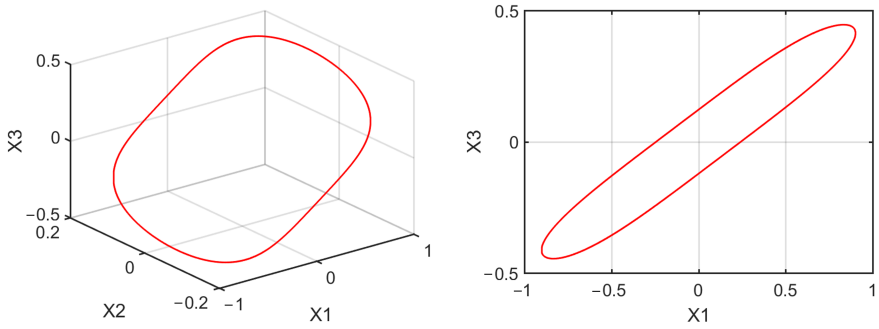


Figure A1. Periodic-1 motion of $\sigma_2 = 3.3647$.

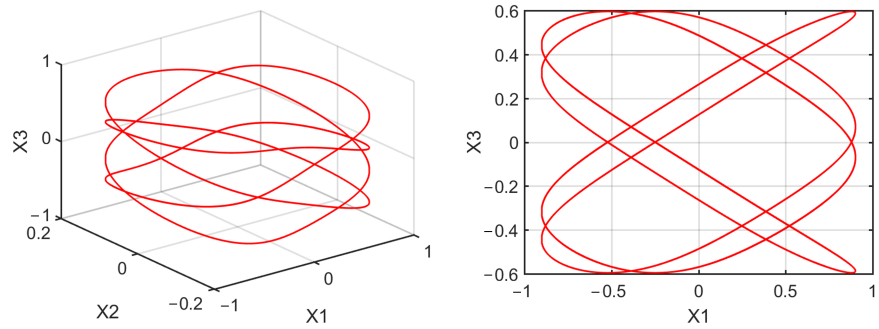


Figure A2. Periodic-4 motion of $\sigma_2 = 1.0011$.

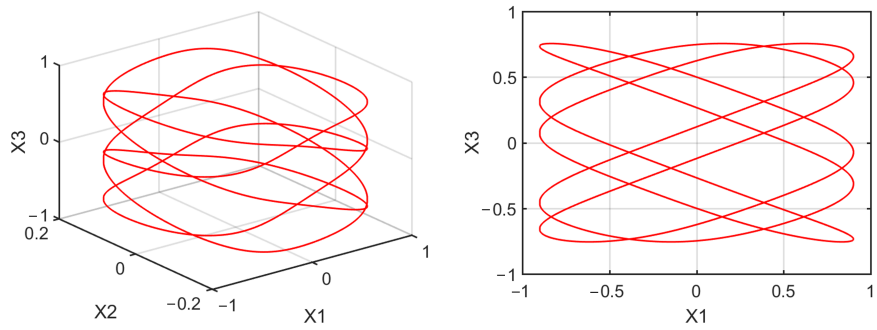


Figure A3. Periodic-5 motion of $\sigma_2 = 0.3124$.

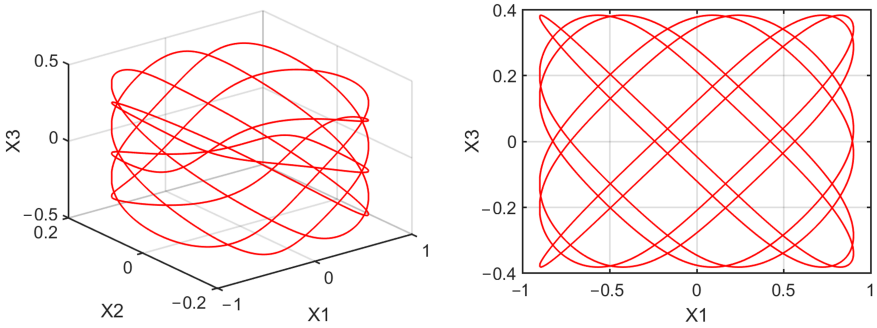


Figure A4. Periodic-6 motion of $\sigma_2 = 6.2567$.

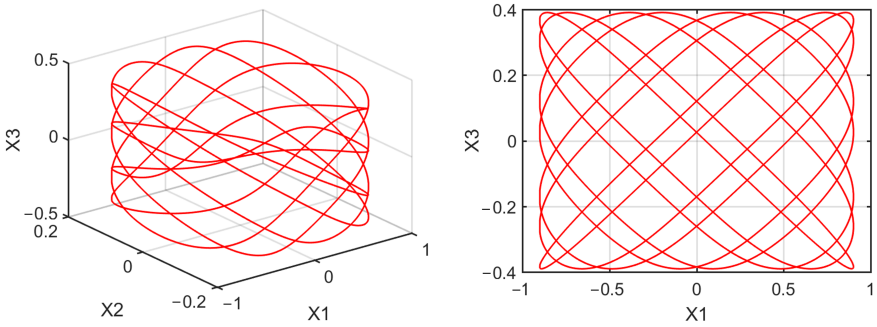


Figure A5. Periodic-7 motion of $\sigma_2 = 5.7615$.

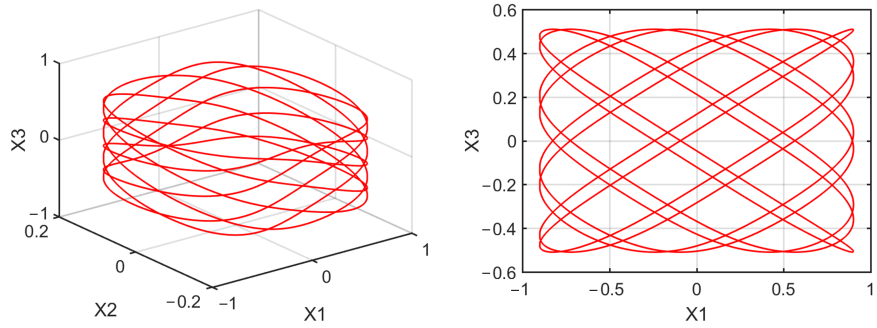


Figure A6. Periodic-8 motion of $\sigma_2 = 1.9433$.

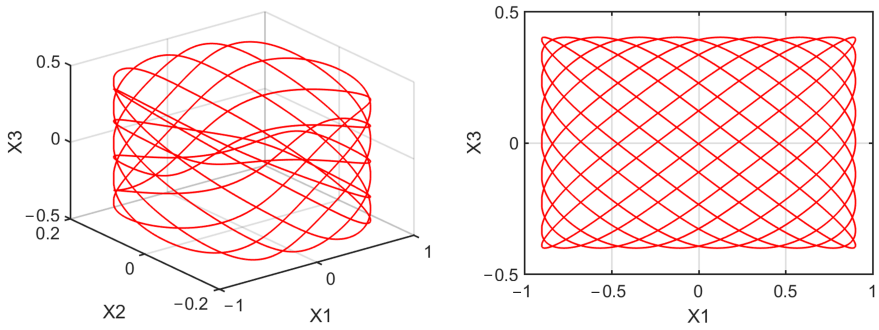


Figure A7. Periodic-9 motion of $\sigma_2 = 5.1468$.

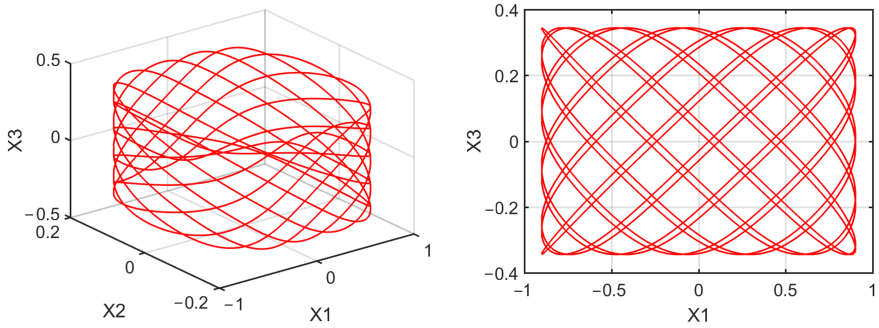


Figure A8. Periodic-10 motion of $\sigma_2 = 9.6206$.

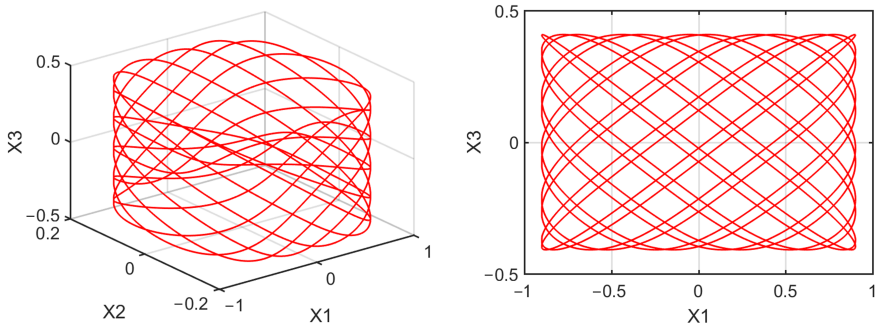


Figure A9. Periodic-11 motion of $\sigma_2 = 4.7810$.

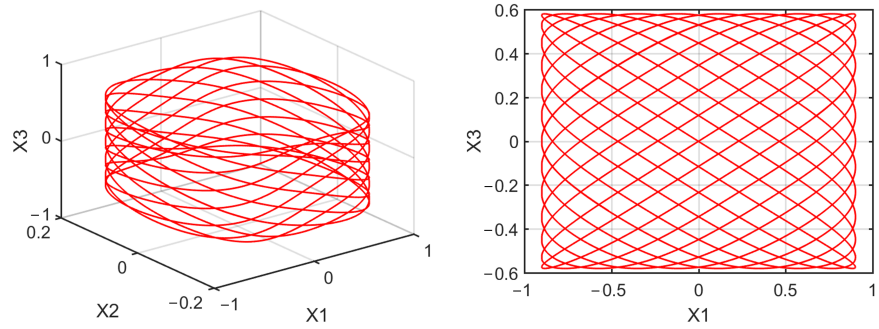


Figure A10. Periodic-13 motion of $\sigma_2 = 1.1199$.

Appendix A.4. Multiple Periodic Motions when σ_1 Is the Free Parameter ($\sigma_2 = 0.67$)

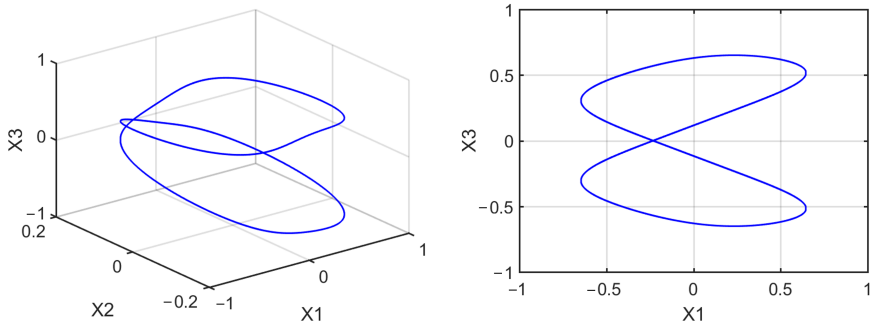


Figure A11. Periodic-2 motion of $\sigma_1 = 2.9801$.

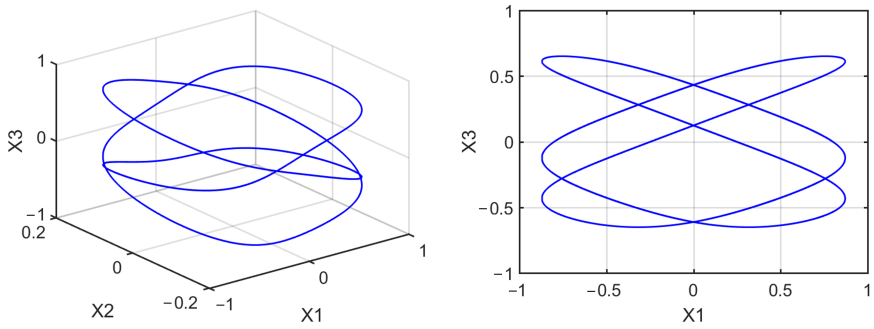


Figure A12. Periodic-3 motion of $\sigma_1 = 0.7983$.

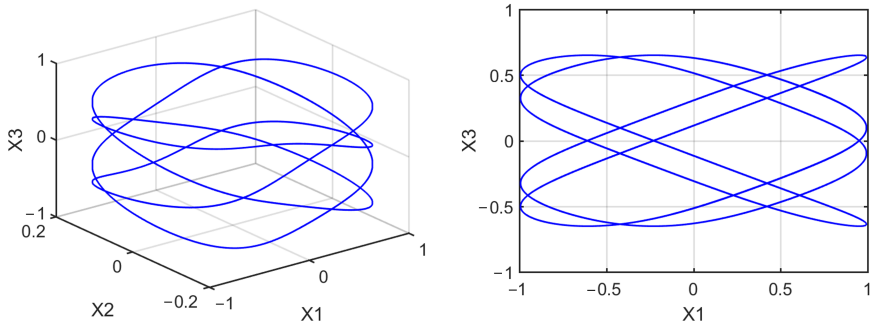


Figure A13. Periodic-4 motion of $\sigma_1 = 0.3811$.

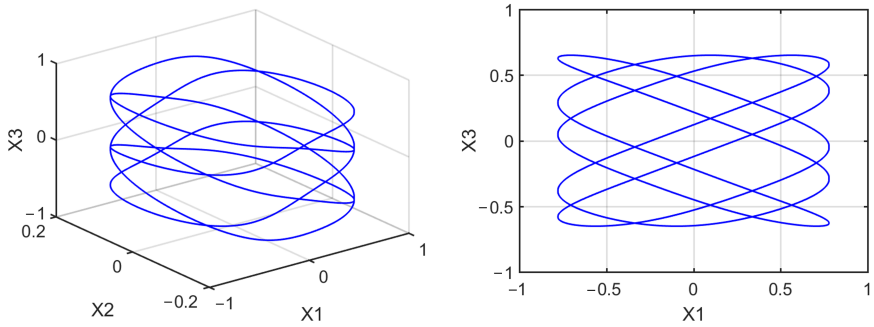


Figure A14. Periodic-5 motion of $\sigma_1 = 1.3432$.

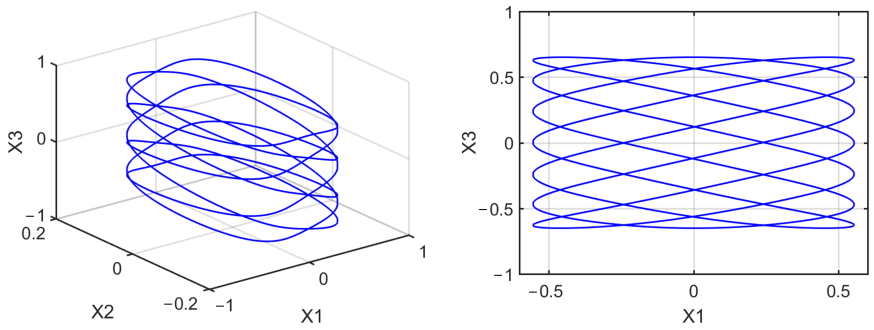


Figure A15. Periodic-7 motion of $\sigma_1 = 5.6284$.

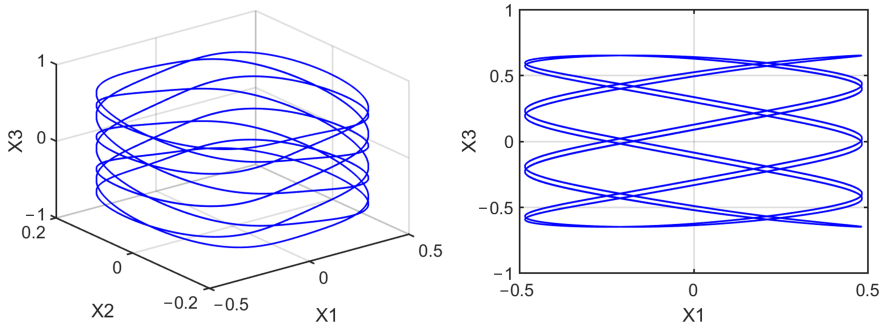


Figure A16. Periodic-8 motion of $\sigma_1 = 9.6648$.

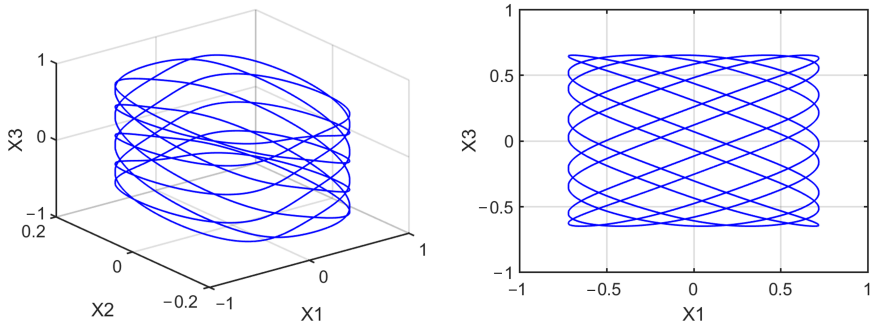


Figure A17. Periodic-9 motion of $\sigma_1 = 1.8987$.

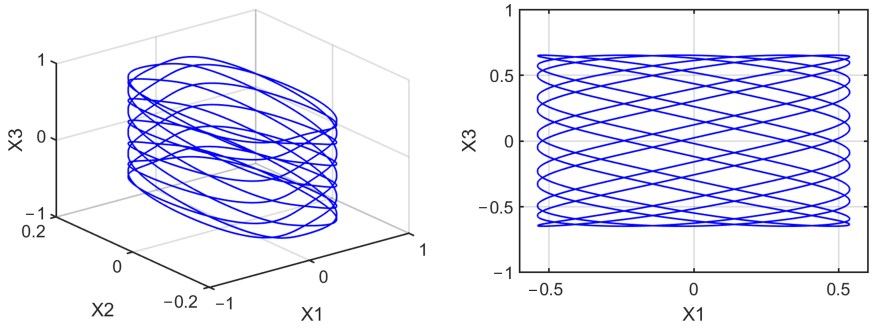


Figure A18. Periodic-12 motion of $\sigma_1 = 6.3116$.

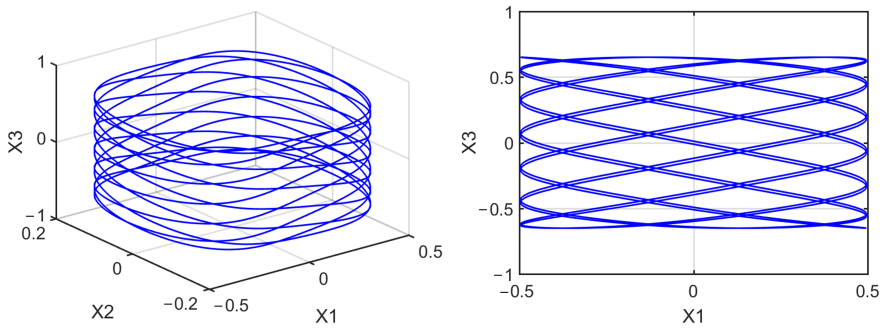


Figure A19. Periodic-13 motion of $\sigma_1 = 8.7295$.

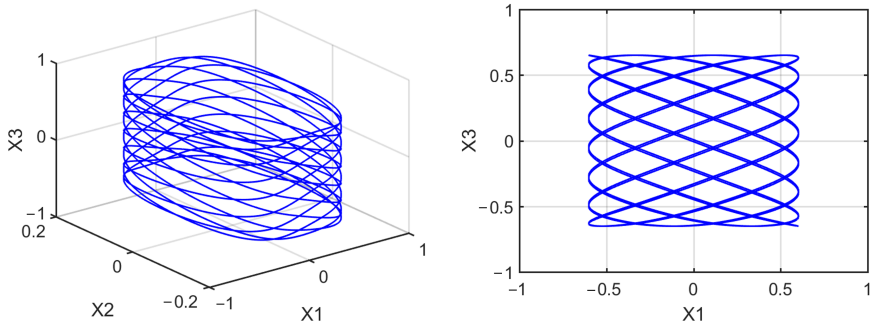


Figure A20. Periodic-15 motion of $\sigma_1 = 3.9695$.

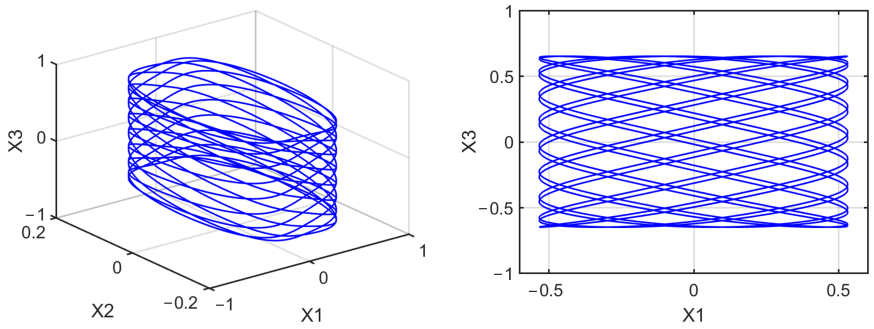


Figure A21. Periodic-17 motion of $\sigma_1 = 6.6229$.

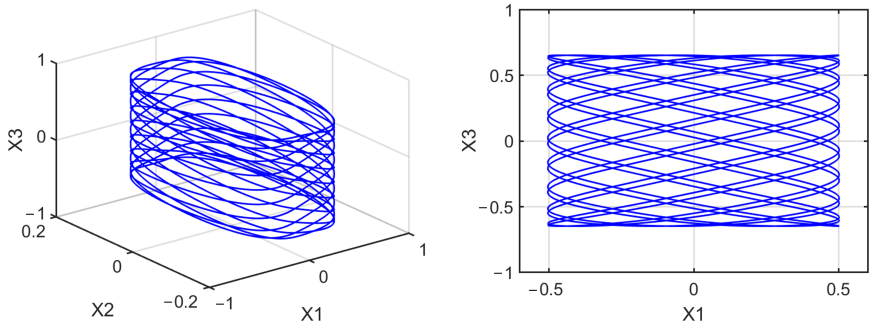


Figure A22. Periodic-18 motion of $\sigma_1 = 8.3480$.

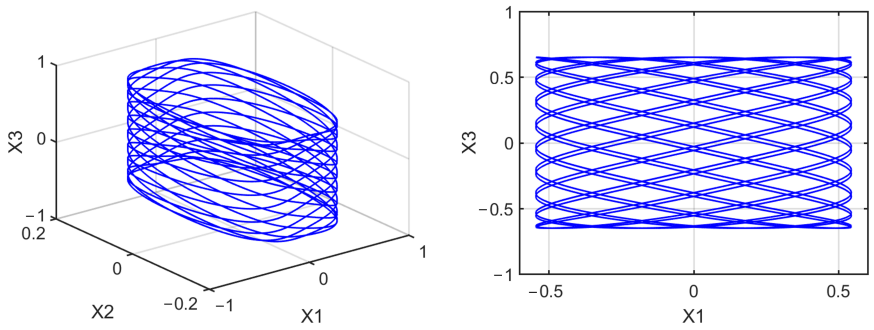


Figure A23. Periodic-19 motion of $\sigma_1 = 6.0491$.

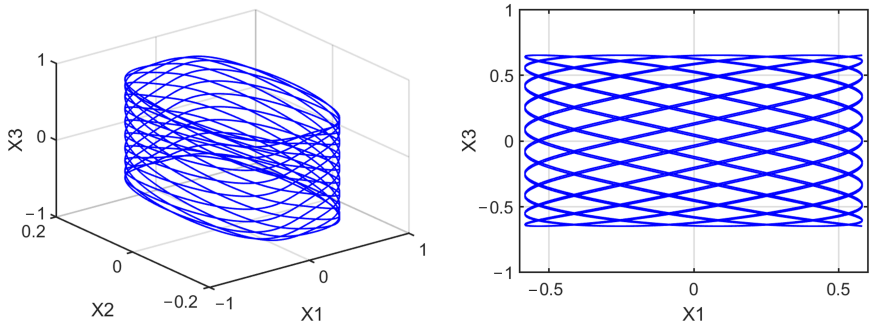


Figure A24. Periodic-20 motion of $\sigma_1 = 4.6103$.

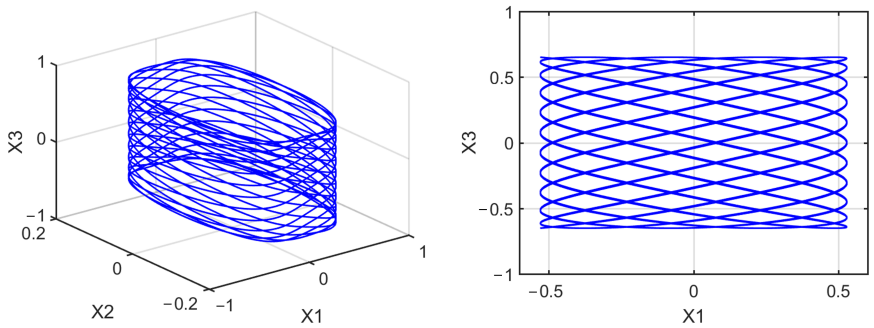


Figure A25. Periodic-22 motion of $\sigma_1 = 6.8000$.

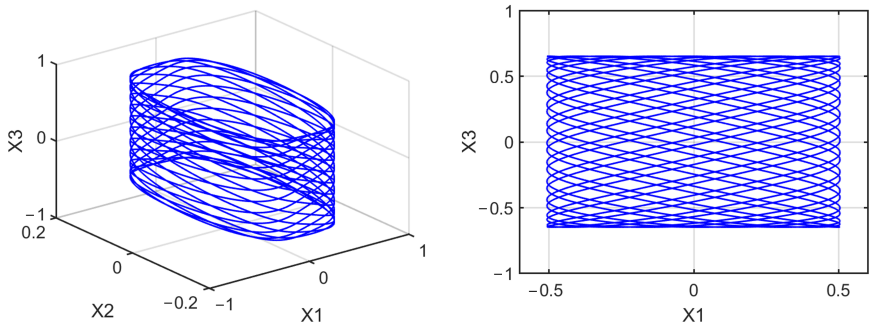


Figure A26. Periodic-23 motion of $\sigma_1 = 8.1412$.

References

1. Inoue, Y. Synthetic chemistry: Light on chirality. *Nature* **2005**, *436*, 1099–1100. [CrossRef] [PubMed]
2. D'Orazio, G. Chiral analysis by nano-liquid chromatograph. *TRAC Trend. Anal. Chem.* **2020**, *125*, 115832. [CrossRef]
3. Cintas, P. *Biochirality Origins, Evolution and Molecular Recognition*; Springer: Berlin/Heidelberg, Germany, 2013
4. Brown, J.M.; Davies, S.G. Chemical asymmetric synthesis. *Nature* **1989**, *342*, 631–636. [CrossRef]

5. Wnendt, S.; Zwingenberger, K. Thalidomide's chirality. *Nature* **1997**, *385*, 303–304. [CrossRef] [PubMed]
6. Yan, X.; You, X.Z.; Sugiyama, H.; Umano, T.; Tanaka, K. (P)-helicene displays chiral selection in binding to Z-DNA. *J. Am. Chem. Soc.* **2004**, *126*, 6566–6567.
7. Yamamoto, T.; Yamada, T.; Nagata, Y.; Suginome, M. High-molecular-weight polyquinoxaline-based helically chiral phosphine (PQXphos) as chirality-switchable, reusable, and highly enantioselective monodentate ligand in catalytic asymmetric hydrosilylation of styrenes. *J. Am. Chem. Soc.* **2010**, *132*, 7899–7901. [CrossRef] [PubMed]
8. Svirko, Y.P.; Zheludev, N.I. *Polarization of Light in Nonlinear Optics*; Wiley: London, UK, 1998.
9. Yin, X.H.; Schäferling, M.; Metzger, B.; Giessen, H. Interpreting chiral nanophotonic spectra: The plasmonic Born-Kuhn model. *Nano Lett.* **2013**, *13*, 6238–6243. [CrossRef]
10. Schäferling, M. *Chiral Nanophotonics: Chiral Optical Properties of Plasmonic Systems*; Springer Nature: Cham, Switzerland, 2017.
11. Wang, X.O.; Li, J.Q.; Li, C.F. Hyperpolarizabilities of chiral molecules based on three-coupled-oscillator model. *Chin. Phys. Lett.* **2004**, *21*, 2433–2436.
12. Gui, L.L.; Hentschel, M.; Defrance, J.; Krauth, J.; Weiss, T.; Giessen, H. Nonlinear Born-Kuhn analog for chiral plasmonics. *ACS Photonics* **2019**, *6*, 3306–3314. [CrossRef]
13. Peyrard, M. Nonlinear dynamics and statistical physics of DNA. *Nonlinearity* **2004**, *17*, R1–R40. [CrossRef]
14. Teif, V.B.; Bohinc, K. Condensed DNA: Condensing the concepts. *Prog. Biophys. Mol. Biol.* **2011**, *105*, 208–222. [CrossRef] [PubMed]
15. Cherstvy, A.G.; Kornyshev, A.A. DNA Melting in Aggregates: Impeded or Facilitated? *J. Phys. Chem. B* **2005**, *109*, 13024–13029. [CrossRef] [PubMed]
16. Leine, R.I. The historical development of classical stability concepts: Lagrange, poisson and lyapunov stability. *Nonlinear Dynam.* **2010**, *59*, 173–182. [CrossRef]
17. Shamash, Y. Comments on the Routh-Hurwitz criterion. *IEEE Trans. Automat. Contr.* **1980**, *25*, 132–133. [CrossRef]
18. Ho, M.T.; Datta, A.; Bhattacharyya, S.P. An elementary derivation of the Routh-Hurwitz criterion. *IEEE Trans. Automat. Contr.* **1998**, *43*, 405–409.
19. Shcherbakov, P.S. Alexander mikhailovitch Lyapunov: On the centenary of his doctoral dissertation on stability of motion. *Automatica* **1992**, *28*, 865–871. [CrossRef]
20. Bacciott, A.; Rosie, L. *Liapunov Functions and Stability in Control Theory*; Springer: London, UK, 2001.
21. Zhang, L.; Chen, F.Q. Bifurcations and stability analysis for nonlinear oscillations of an airfoil. *Chaos Soliton. Fract.* **2017**, *103*, 220–231. [CrossRef]
22. Wang, X.R.; Kampen, E.V.; Chu, Q.P.; Lu, P. Stability analysis for incremental nonlinear dynamic inversion control. *J. Guid. Control Dynam.* **2019**, *42*, 1116–1129. [CrossRef]
23. Santana, M.; Gonalves, P.; Silveira, R. Nonlinear oscillations and dynamic stability of an elastoplastic pyramidal truss. *Nonlinear Dynam.* **2019**, *98*, 2847–2877. [CrossRef]
24. Hategekimana, F.; Saha, S.; Chaturvedi, A. Dynamics of amoebiasis transmission: Stability and sensitivity analysis. *Mathematics* **2017**, *5*, 58. [CrossRef]
25. Zhang, J.M.; Zhang, L.J.; Bai, Y.Z. Stability and bifurcation analysis on a predator-prey system with the weak Allee effect. *Mathematics* **2019**, *7*, 432. [CrossRef]
26. Li, J.B. Hilbert's 16th problem and bifurcations of planar polynomial vector fields. *Int. J. Bifurcat. Chaos* **2003**, *13*, 47–106. [CrossRef]
27. Quan, T.T.; Li, J.; Zhang, W.; Sun, M. Bifurcation and number of subharmonic solutions of a 2n-dimensional non-autonomous system and its application. *Nonlinear Dynam.* **2019**, *98*, 301–315. [CrossRef]
28. Quan, T.T.; Li, J.; Zhu, S.T.; Sun, M. Bifurcation and number of periodic solutions of some 2n-dimensional systems and its application. *J. Dyn. Differ. Equ.* **2021** . [CrossRef]
29. Barreira, L.; Llibre, J.; Valls, C. Bifurcation of limit cycles from a 4-dimensional center in R^m in resonance 1:N. *J. Math. Anal. Appl.* **2012**, *389*, 754–768. [CrossRef]
30. Barreira, L.; Llibre, J.; Valls, C. Limit cycles bifurcating from a zero-Hopf singularity in arbitrary dimension. *Nonlinear Dynam.* **2018**, *92*, 1159–1166. [CrossRef]
31. Sun, M.; Zhang, W.; Chen, J.E.; Yao, M.H. Subharmonic Melnikov theory for degenerate resonance systems and its application. *Nonlinear Dynam.* **2017**, *89*, 1173–1186. [CrossRef]
32. Kadry, S.; Alferov, G.; Ivanov, G.; Korolev, V.; Selitskaya, V. A new method to study the periodic solutions of the ordinary differential equations using functional analysis. *Mathematics* **2019**, *7*, 677. [CrossRef]
33. Li, J.; Quan, T.T.; Zhang, W. Bifurcation and number of subharmonic solutions of a 4D non-autonomous slow-fast system and its application. *Nonlinear Dynam.* **2018**, *92*, 721–739. [CrossRef]
34. Li, J.; Zhang, L.N.; Wang, D. Unique normal form of a class of 3 dimensional vector fields with symmetries. *J. Differ. Equ.* **2014**, *257*, 2341–2359. [CrossRef]